

# Alkali Bose Condensate Mixtures

Tin-Lun Ho and V.B. Shenoy

*Physics Department, The Ohio State University, Columbus, Ohio 43210*

## Abstract

We show that binary mixtures of Bose-condensates of alkali atoms have a great variety of ground state and vortex structures which can be accessed experimentally by varying the particle numbers of different alkalis. We have constructed a simple algorithm to determine the density profiles of these states, and have worked out their phase diagrams within Thomas-Fermi approximation. Many structures of the alkali binary contain a coexisting region, which is the analog of the long sought  $^3\text{He}$ - $^4\text{He}$  interpenetrating superfluids in ultra-low temperature physics.

The search of Bose condensate in alkali atoms [1] [2] [3] has a deep root in ultra-low temperature physics. Since the discovery of superfluid  $^3\text{He}$ , the searches of the next elemental superfluid have been focusing on spin polarized hydrogen and  $^3\text{He}$ - $^4\text{He}$  mixture. The former promises another Bose superfluid besides the only known example of  $^4\text{He}$ , the latter, the first example of interpenetrating superfluids. The recent discoveries of alkali Bose condensates [1] [2] [3] have in essence achieved the goal of the superfluid hydrogen search. Since there are no intrinsic difficulties in loading more than one alkali element and have them cooled in the same trap, it appears highly promising that interpenetrating superfluids may be realized for the first time within the same experimental setting.

In this paper, we shall discuss binary mixtures of alkali condensates. Such mixtures may consist of different alkalis such as  $^{87}\text{Rb}$ - $^{23}\text{Na}$ , or different isotopes such as  $^{87}\text{Rb}$ - $^{85}\text{Rb}$ , or different hyperfine states of the same alkali such as the ( $F = 2, M_F = 2$ ) and ( $F = 1, M_F = 1$ ) states of  $^{87}\text{Rb}$ . We shall denote the two different alkalis as 1 and 2, and their

particle numbers as  $N_1$  and  $N_2$ . Unlike single component systems which are characterized by a single scattering length, alkali binaries are characterized by three scattering lengths  $a_1, a_2$ , and  $a_{12}$ ; representing interactions between like and unlike alkalis. (While scattering lengths of like alkalis are known at present, those of unlike alkalis are not). As we shall see, this moderate increase in energy scales leads to a proliferation of ground state and vortex structures, which we shall illustrate for the case  $a_1, a_2 > 0$ . This case is chosen because it has the greatest structural diversity, and can be analysed by simple analytic methods. The results for this case will also be useful in understanding the qualitative features of other (negative scattering length) cases.

Our key results are : (a) a simple algorithm for determining the density profiles of the binary mixtures, (b) the phase diagrams of the vortex free ground states [denoted as  $(\mathbf{v0})$ ], and the vortex states in either 1 or 2 [denoted as  $(\mathbf{v1})$  and  $(\mathbf{v2})$  respectively]. We limit our discussions to these two types of vortices because they are the states the system will first fall into as the confining potential is rotated. Our algorithm, however, can be applied to arbitrary number of vortices in 1 and 2. As we shall see, the structure of the mixture depends on two parameters  $\alpha$  and  $\beta$ , which are proportional to the strength of  $a_{12}$  and the relative strength between  $a_1$  and  $a_2$  respectively. These parameters determine whether alkali 2 when added to an existing cloud of 1 will stay at its exterior or interior. Many structures of the mixture contain a coexisting region which is especially large when  $N_1 \sim N_2$ . This is the analog of the long sought  $^3\text{He}$ - $^4\text{He}$  superfluid mixture in ultra-low temperature physics. Even greater structural diversity is found when vortices are inserted in one of the alkalis. When the alkali 1 and 2 are mutually repulsive,  $a_{12} > 0$ , the vortex free alkali (say, 2) always enter the vortex core of 1, giving rise to a variety of “vortex donut” structures in 1. When  $a_{12} < 0$ , one has an unusual “concentric donut” structure where a vortex free “donut” of 2 embedded in a “vortex donut” of 1.

Our results are obtained by minimizing the Gross-Piteavskii energy  $E(\Psi_1, \Psi_2) = T + V$  subject to the constraint of constant particle numbers, i.e. by the condition  $\delta K = 0$ ,  $K \equiv E(\Psi_1, \Psi_2) - \mu_1 N_1 - \mu_2 N_2$ , where  $(\Psi_i, \mu_i)$  are the order parameter and chemical potential

of the  $i$ -th alkali,  $i = 1, 2$ . The potential energy  $V$  and kinetic energy  $T$  are

$$V = \sum_{i=1,2} \int \left( U_i(\mathbf{x}) |\Psi_i|^2 + \frac{2\pi\hbar^2 a_i}{M_i} |\Psi_i|^4 \right) + \int \frac{2\pi\hbar^2 a_{12}}{\sqrt{M_1 M_2}} |\Psi_1|^2 |\Psi_2|^2 \quad (1)$$

$$T = \int \left( \sum_{i=1,2} \frac{\hbar^2 |\nabla \Psi_i|^2}{2M_i} + \zeta_1 \Psi_1^* \nabla \Psi_1 \cdot \Psi_2^* \nabla \Psi_2 + \zeta_2 \Psi_1^* \nabla \Psi_1 \cdot \Psi_2 \nabla \Psi_2^* + c.c. \right). \quad (2)$$

$U_i$  is the potential of the magnetic trap for the  $i$ -th alkali, generally of the form [4]  $U_i(\mathbf{x}) = \frac{g_i \mu_B B_o}{2L^2} (r^2 + \lambda^2 z^2) \equiv \frac{1}{2} M_i \omega_i^2 (r^2 + \lambda^2 z^2)$ , where  $g_i$  and  $M_i$  are the g-factor and mass of the  $i$ -th alkali,  $\mu_B$  is the Bohr magneton,  $B_o$  is the magnetic field at the center of the trap,  $L$  is the length scale of the variations of the magnetic field, and  $\lambda$  is the trap anisotropy.  $\zeta_1$  and  $\zeta_2$  are complex coefficients which is caused by back flow effects between different alkalis. They are expected to be small in the dilute limit.

Our calculations are performed within the Thomas-Fermi approximation (TFA), which is a good approximation in the limit of large number of particles, as pointed out by Baym and Pethick [5]. In TFA, one ignores all  $\nabla |\Psi_i|$  terms in  $T$ . For vortex free structures ( $\mathbf{v}\mathbf{0}$ ), this amounts to setting  $T = 0$ . For ( $\mathbf{v}\mathbf{1}$ ) vortices, ( $\Psi_1 = |\Psi_1| e^{i\phi}$  and  $\Psi_2 = |\Psi_2|$ ), TFA amounts to retaining only the centrifugal term  $|\Psi_1|^2/r^2$  in  $T$ . Because of the absence of gradient terms  $\nabla |\Psi_i|$ , the densities obtained from TFA usually consist of discontinuities in radial curvature. Such changes in curvature in fact take place smoothly over the distance of correlation length, which decreases with increasing particle numbers [5]. It is convenient to write  $K$  and  $N_i$  in dimensionless form by the following rescaling: (i)  $z \rightarrow z/\lambda$ , (ii)  $\mathbf{x} \rightarrow a_T \mathbf{x}$ , where  $\hbar^2/M_1 a_T^4 = g_1 \mu_B B_o/L^2$ , (iii)  $|\Psi_i|^2 = A_i \rho_i$ , where  $A_1 = M_1 \omega_1 / (8\pi \hbar a_1)$ ,  $A_2/A_1 = (a_1 M_2 / a_2 M_1)^{1/2}$ , (iv)  $\mu_1 \equiv \frac{1}{2} \hbar \omega_1 \nu_1$  and  $\mu_2 \equiv \frac{1}{2} \hbar \omega_1 (A_2/A_1) \nu_2$ , (v)  $K \equiv (\hbar \omega_1 / 4\lambda) (a_T / (4\pi a_1)) \mathcal{K}$ . (vi)  $N_1 = (8\pi\lambda)^{-1} (a_T/a_1) n_1$ ,  $N_2 = (8\pi\lambda)^{-1} (a_T/a_1) \sqrt{a_1 M_2 / a_2 M_1} n_2$ . We then have

$$\mathcal{K} = \int d^3x \left[ -c_1 \rho_1 - c_2 \rho_2 + \frac{1}{2} (\rho_1^2 + \rho_2^2 + 2\alpha \rho_1 \rho_2) \right], \quad n_i = \int d^3x \rho_i \quad (3)$$

$$c_1(\mathbf{x}) = \nu_1 - \left( r^2 + \frac{p}{r^2} + z^2 \right) \quad c_2(\mathbf{x}) = \nu_2 - \beta (r^2 + z^2), \quad (4)$$

where  $\mathbf{x} = (\mathbf{r}, z) = (x, y, z)$  in eq.(4), and  $p = 0$  and  $1$  for  $(\mathbf{v0})$  and  $(\mathbf{v1})$  state respectively.  $\alpha$  and  $\beta$  are defined as

$$\alpha = \frac{a_{12}}{2\sqrt{a_1 a_2}}, \quad \beta = \frac{g_2}{g_1} \sqrt{\frac{a_1 M_2}{a_2 M_1}}, \quad (5)$$

reflecting the interaction between unlike alkalis, and the relative strength of the self interaction between like alkalis. For  $(\mathbf{v2})$  vortices, the energy can be rescaled to the same form as eq.(3) with the same  $\alpha$  and  $\beta$  in eq.(5), and with  $(c_1=r^2 + z^2 - \nu_1, c_2=\beta(r^{-2} + r^2 + z^2) - \nu_2)$  [6]. We shall not consider the case  $(\alpha < -1)$ , which does not have bulk stability. In our subsequent illustrations, we use the example of  $^{87}\text{Rb}$ - $^{23}\text{Na}$  mixture, (our alkali 1 and 2), which has identical  $g$  factors. We thus have  $a_1 \approx 100\text{\AA}$  [1],  $a_2 \approx 49\text{\AA}$  [3], and  $\beta = 0.73$ . Since  $a_{12}$  is not known for this mixture, we consider the entire range of  $\alpha > -1$ . Taking  $\lambda = 1$  and  $a_T = 4 \times 10^{-4}\text{cm}$ , we have  $N_1 = 16.7n_1, N_2 = 12.3n_2$ .

Our goal is to find the condensate structure (i.e.  $\rho_1, \rho_2$ ) as a function of particle number  $n_1, n_2$ . This is done by : **(I)** Minimizing  $\mathcal{K}$  to find the equilibrium densities  $\rho_i$  for given chemical potential  $\nu_i$ , **(II)** substituting these densities into eq.(3) to obtain the relation  $n_i = n_i(\nu_1, \nu_2)$ , **(III)** inverting this relation to obtain  $\nu_i = \nu_i(n_1, n_2)$  and hence the evolution of  $\rho_i$  (through their dependence on  $\nu_i$ ) as a function of  $n_i$ . Although much of our labor went into **(II)** and **(III)**, they are straightforward (though lengthy) calculations once the densities profiles are determined by the simpler but subtler step **(I)**, which we now explain.

Let **[0]**, **[1]**, **[2]**, **[12]** denote the vacuum, the single phase of 1, 2, and the coexisting phase of 1 and 2 respectively. Their densities are given by the stationary conditions of  $\mathcal{K}$ ,

$$\mathbf{[12]} : \rho_1 = \frac{c_1 - \alpha c_2}{1 - \alpha^2} \geq 0, \quad \rho_2 = \frac{c_2 - \alpha c_1}{1 - \alpha^2} \geq 0; \quad \mathbf{[0]} : \rho_1 = \rho_2 = 0; \quad (6)$$

$$\mathbf{[1]} : \rho_1 = c_1 \geq 0, \quad \rho_2 = 0, \quad \mathbf{[2]} : \rho_2 = c_2 \geq 0, \quad \rho_1 = 0. \quad (7)$$

The distribution of these ‘‘phases’’ in  $c_1$ - $c_2$  plane will be referred to the *distribution plot*, which depends only on  $\alpha$ . The distribution plots for  $(0 < \alpha < 1)$  and  $(-1 < \alpha < 0)$  are shown in fig.(1.1) and fig.(1.3). [The distribution plot for  $(\alpha > 1)$  will not be shown

as it is given by fig.(1.1) with the coexisting region **[12]** collapsed into the line  $c_1 = c_2$ . The boundaries separating **[12]** from **[2]** and **[1]** are denoted as  $\mathbf{1}_o$  and  $\mathbf{2}_o$ . They are the surfaces of vanishing  $\rho_1$  and  $\rho_2$ , described by equations ( $\mathbf{1}_o : c_1 = \alpha c_2$ ) and ( $\mathbf{2}_o : c_2 = \alpha c_1$ ) respectively. The boundaries separating **[0]** from **[1]** and **[2]** are denoted as  $\mathbf{1}^o$  and  $\mathbf{2}^o$ . They are described by equations ( $\mathbf{1}^o : c_1 = 0$ ) and ( $\mathbf{2}^o : c_2 = 0$ ). From eq.(4), one can see that a path in real space will have an “image” path in  $c_1$ - $c_2$  space. For example, the image of a radial path on the horizontal plane with height  $z$  is given by  $\Gamma(z) : c_1 - \nu_1(z) = \beta^{-1}[c_2 - \nu_2(z)] + p\beta[c_2 - \nu_2(z)]^{-1}$ , where  $\nu_1(z) = \nu_1 - z^2$ ,  $\nu_2(z) = \nu_2 - \beta z^2$ . For vortex free state ( $p = 0$ ),  $\Gamma(z)$  is a straight line with slope  $\beta$  emerging from the point  $(\nu_1(z), \nu_2(z))$ , which is shown as a dashed line emerging from a circle in fig.(1.1). For the **(v1)** vortices,  $\{\Gamma(z)\}$  is a family of curves shown in fig.(1.2), where  $z_2 > z_1 > 0$  in this figure. The arrows on these paths indicate the direction of increasing  $r$ . As  $r$  varies from 0 to  $\infty$ ,  $\Gamma(z)$  intersects the phase boundaries in a specific order. From the definition of  $\nu_i(z)$ , it is easy to see that as  $|z|$  increases,  $\Gamma(z)$  slides down rigidly along the straight line with slope  $\beta$ .

The above considerations suggest a simple algorithm for determining the structure of the alkali binary : (i) For given  $\nu_1, \nu_2$ , draw the image paths  $\{\Gamma(z)\}$  on the distribution plot.  $\Gamma(z)$  will intersect a set of phase boundaries in a specific order. (ii) Construct the set of boundary surfaces intersected by  $\{\Gamma(z)\}$ . (iii) Eliminate all portions of the boundary surfaces that are inconsistent with the order of intersections generated in (i). The remaining surfaces are the physical boundaries in the mixture. The densities of various phases bounded by these surfaces are given by eq.(6) and (7).

To illustrate this algorithm, consider the vortex free mixture in fig.(1.1). The image paths of this mixture intersect phase boundaries  $\mathbf{2}_o, \mathbf{1}_o$  and  $\mathbf{2}^o$ , corresponding to a set of concentric spherical surfaces in real space separating the single component and coexisting regions as shown in fig.(1.4). Fig.(1.4) is the structure of the mixture. For the **(v1)** vortex in fig.(1.2), the family  $\{\Gamma(z)\}$  intersects all four phase boundaries ( $\mathbf{1}_o, \mathbf{2}_o, \mathbf{1}^o, \mathbf{2}^o$ ) in the order ( $\mathbf{1}_o \mathbf{2}_o \mathbf{1}^o$ ), or  $\mathbf{2}^o$  alone. Displaying all four boundary surfaces as in fig.(1.5) and eliminating all sections of these surfaces inconsistent with the order of intersection, we obtain the physical

boundaries shown in fig.(1.6). The densities of the phases  $[1]$ ,  $[12]$ , and  $[2]$  enclosed by these surfaces are given in eq.(6) and (7). It is clear that this algorithm applies to mixtures with arbitrary number of vortices in 1 and 2, which have different image trajectories.

Having determined the density profiles for given chemical potential  $(\nu_1, \nu_2)$ , we have followed the aforementioned Steps **(II)** and **(III)** to construct the phase diagrams for both ground states  $[(\mathbf{v0})]$  and vortex states  $[(\mathbf{v1})$  and  $(\mathbf{v2})]$  over the entire range of  $(\alpha, \beta)$ . For reasons to be explained shortly, we shall focus on the parameter range [**A**:  $0 < \alpha < 1, \beta < \alpha$ ], [**B**:  $0 < \alpha < 1, \alpha < \beta < 1$ ], and [**C**:  $-1 < \alpha < 0, \beta < 1$ ]. For brevity, we shall denote the  $(\mathbf{v0})$  state of **A** as  $(\mathbf{v0})\text{-A}$ , the  $(\mathbf{v2})$  state of **B** as  $(\mathbf{v2})\text{-B}$ , etc. As it turns out, for ground state phase diagrams, it is sufficient to discuss those of  $(\mathbf{v0})\text{-A}$  and  $(\mathbf{v0})\text{-B}$ . For vortex phase diagrams, it is sufficient to discuss those of  $(\mathbf{v1})\text{-A}$ ,  $(\mathbf{v2})\text{-A}$ ,  $(\mathbf{v1})\text{-B}$ , and  $(\mathbf{v1})\text{-C}$ . The phase diagrams of all other cases can be obtained from these either by interchanging 1 and 2 or by collapsing the coexistence region down to a line [7]. In all cases we have studied, the condensate structure evolves *continuously* over the entire  $n_1\text{-}n_2$  space, even though the phase diagrams may contain different structural regimes.

The typical phase diagrams of  $(\mathbf{v0})\text{-A}$  and  $(\mathbf{v0})\text{-B}$  are shown in fig.(2.1) and (2.2), with  $(\alpha = 0.9, \beta = 0.73)$  and  $(\alpha = 0.6, \beta = 0.73)$  respectively. The density profiles for mixtures marked by letters “a” to “g” in fig.(2.1) and (2.2) are shown in fig.(2.3) to (2.9). The line between *b* and *c* in fig.(2.1) divides the configurations where 2 is absent or present at the origin. The main difference between **A** and **B** is that the former ( $\beta < \alpha$ ) represents a regime where repulsion between unlike alkalis dominates. As a result, when a small amount of 2 is added to an existing condensate of 1, it stays at its surface in the case of **A** (see fig.(2.3) and (2.4)), whereas it enters directly into the center of 1 in the case of **B** (see fig.(2.7)). One can see from fig.(2.5) and (2.8) that when 1 and 2 have similar number of particles, the coexisting region of 1 and 2 occupies a substantial portion of the mixture. This large coexisting region is the analog of the long sought interpenetrating superfluid phase in  $^3\text{He}\text{-}^4\text{He}$  mixture.

Next, we turn to the vortex states. The presence of a vortex (say, in alkali 1) will turn the spherical ground state condensate into a vortex “donut”. The donut hole is the vortex

core, around which supercurrent circulates. For repulsive interactions, ( $\alpha > 0$ ), the general behavior of the (vortex free) alkali 2 is to fill up the vortex core and to penetrate into the interior of vortex 1. The typical phase diagram of **(v1)-A**, **(v2)-A**, and **(v1)-B** are shown in fig.(3.1), (3.5), and (3.7) respectively, with values of ( $\alpha = 0.9, \beta = 0.73$ ) for **A** and ( $\alpha = 0.6, \beta = 0.73$ ) for **B**. The scales of  $n_1$  and  $n_2$  are chosen so that a condensate with  $N_1 = N_2 = 10^4$  will appear in the middle of the diagram. There are in fact many more structural regimes near the  $n_1$  and  $n_2$  axes which correspond to various stages of filling up the vortex core. However, they only exist close to the  $n_1$  and  $n_2$  axes (i.e. small number of particles in either 1 or 2) and are not visible on this scale [8].

The boundary surfaces for the mixtures marked as “a” to “f” in fig.(3.1), (3.5) and (3.7) are shown in the rest of figure 3 with self explanatory labelling. These surfaces are presented only in a quadrant of  $r$ - $z$  plane, as they are cylindrical symmetric about  $z$  and have mirror symmetry about the  $xy$  plane. The boundaries **1<sub>o</sub>** and **2<sub>o</sub>** are represented by solid lines, while (**1<sup>o</sup>** and **2<sup>o</sup>**) are represented by dashed lines. 1 and 2 coexist in the region between the dashed lines. The curve in fig.(3.1) between  $a$  and  $b$  divides regions where a ring of single phase [**1**] is present or absent in the interior of the “vortex donut”. The curve between  $b$  and  $c$  divides the regions where the “vortex donut” resides entirely inside or extends beyond the spherical cloud of 2. The phase diagram of **(v2)-A** is very simple as all mixture states have the same qualitative structure shown in fig.(3.6). The phase diagram of **(v1)-B** (fig.(3.7)) is essentially that of **(v1)-A** (fig.(3.1)) with the region occupied by “ $b$ ” is collapsed into a line. The absence of this region is due to the weakness of mutual repulsion between different alkalis (i.e. small  $\alpha$ ), so that alkali 2 always penetrate completely the vortex donut of 1.

Finally, we consider the **(v1)-C** vortices, i.e. the vortex state of a mixture with  $a_{12} < 0$ , (hence  $\alpha < 0$ ). The typical phase diagram is shown in fig.(4.1), (where we have chosen  $\alpha = -0.9, \beta = 0.73$ ). It is qualitatively the same for all values of  $\beta$ . The boundary surfaces of the mixtures marked as  $a$ ,  $b$ , and  $c$  are shown in fig.(4.2) to (4.4). The region in fig.(4.1) containing “ $a$ ” describes the unusual structure of a vortex free donut of 2 is embedded in the vortex donut of 1. When crossing the boundary separating  $a$  and  $b$  in fig.(4.1), the hole

of “donut” 2 shrinks to zero, filling up the vortex core of 1. As one crosses the boundary separating  $b$  and  $c$  in fig.(4.1), the “vortex donut” 1 is completely devoured by 2.

From the above discussions, we see that binary mixtures of alkali Bose condensates possess a great variety of ground state and vortex structures, which can be accessed by varying the number of particles of each alkali. This array of structures allows one to go continuously from a regime of interpenetrating superfluids to one with separated phases. The possibility of scanning through this continuum offers great opportunities to study coupled macroscopic quantum phenomena and interactions of elementary excitations in distinct Bose fluids. Realizations of alkali condensate mixtures will certainly deepen our understanding of interacting Bose fluids, and widen our horizon on superfluid phenomenon.

TLH would like to thank Greg Lafyatis for discussions. This work is supported in part by NSF Grant No. DMR-9406936.

## REFERENCES

- [1] M.H. Anderson, J.R. Ensher, M.R. Mathews, C.E. Weiman, and E.A. Cornell, *Science* **269**, 198 (1995).
- [2] C.C. Bradley, C.A. Sackett, J.J. Tollett, and R.G. Hulet, *Phys. Rev. Lett.* **75**, 1687, (1995).
- [3] K.B. Davis, M.O. Mewes, M.R. Andrews, N.J. van Druten, D.S. Durfee, D.M. Kurn, and W. Ketterle, *Phys. Rev. Lett.* **75**, 3969 (1995).
- [4] See T.L. Ho and V.B. Shenoy, (cond-mat.9603077) for a derivation of this form of potentials in current magnetic traps. For simplicity, we shall consider traps with sufficiently small field gradients so that the spin-gauge effect discussed therein remains small.
- [5] G. Baym and C.J. Pethick, *Phys. Rev. Lett.* **76**, 6 (1996).
- [6] The corresponding rescaling for the **(v2)** case is to change  $a_T$  and  $A_1$  in **(v1)** to  $a_T \rightarrow a_T(M_1g_1/M_2g_2)^{1/4}$ ,  $A_1 \rightarrow A_1(M_1g_1/M_2g_2)^{1/2}$ . This will cause  $n_i$  of **(v1)** to change to  $n_i \rightarrow (M_1g_1/M_2g_2)^{5/4}n_i$ .
- [7] All cases with  $\beta > 1$  can be obtained from those of  $\beta < 1$  by interchanging 1 and 2. All cases with  $\alpha > 1$  can be obtained from those with  $\alpha < 1$  by shrinking the coexistence phase down to a line. The phase diagram of **(v0)-C** is qualitatively the same as **(v0)-B**, (i.e. fig.(2.2)) and need not be discussed separately. Similarly, **(v2)-B** and **(v2)-C** are qualitatively similar to **(v1)-B** and **(v1)-C**, with  $n_1$  and  $n_2$  axes interchanged.
- [8] T.L.Ho and V.B. Shenoy, to be published.

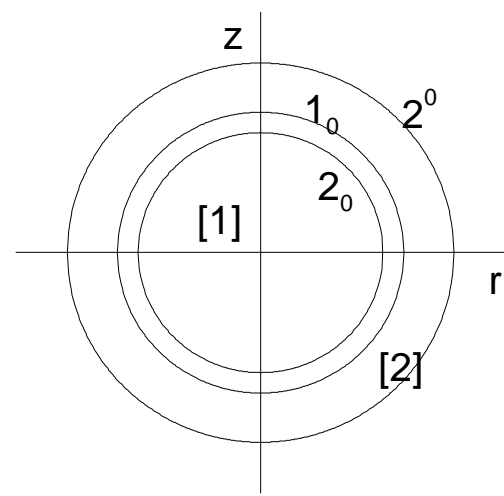
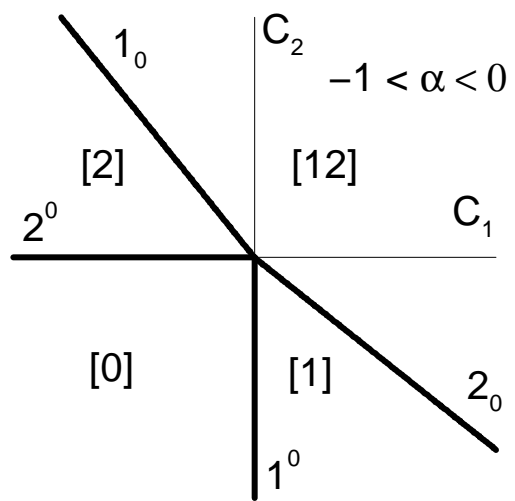
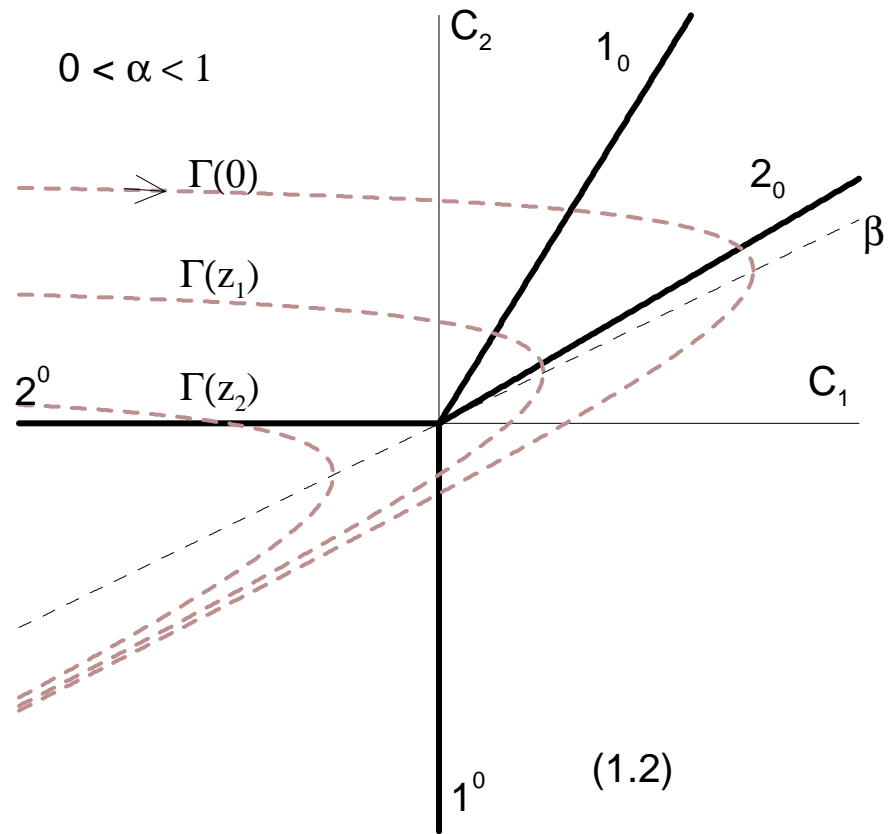
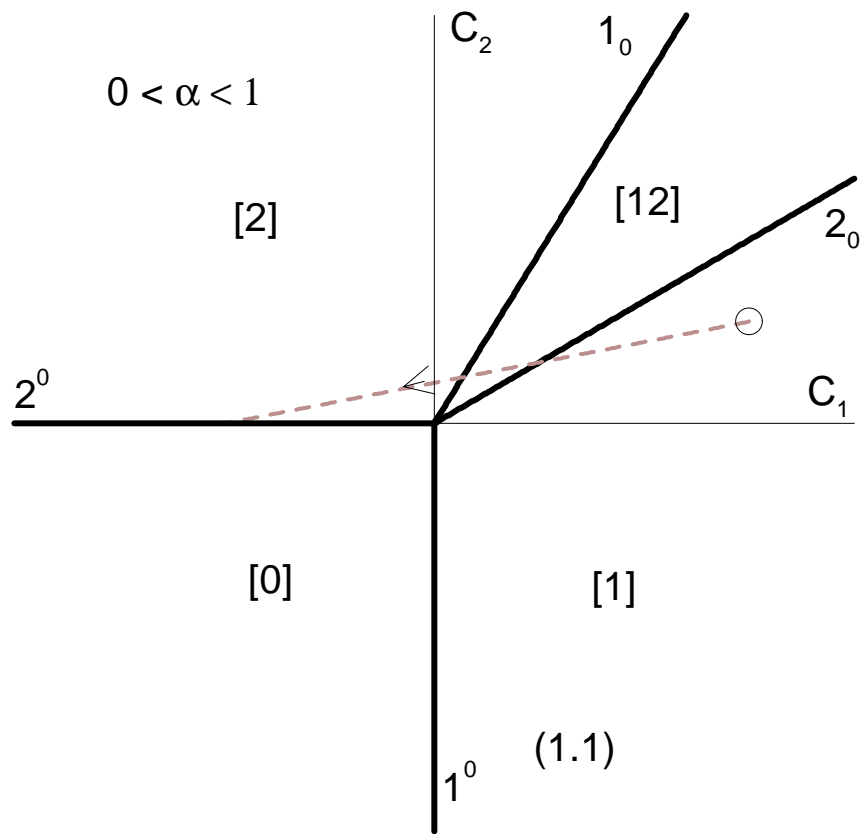
## Caption

**Figure 1:** Fig.(1.1) and (1.2) show the typical distribution plots for  $0 < \alpha < 1$ . The “image trajectories”  $\Gamma(z)$  (dashed lines) of the ground state ( $\mathbf{v0}$ ) and the ( $\mathbf{v1}$ ) vortex of a mixture with chemical potential  $(\nu_1, \nu_2)$  are shown as dashed lines in fig.(1.1) and (1.2). In fig.(1.2),  $z_2 > z_1 > 0$ . Fig.(1.3) shows the distribution plot for  $-1 < \alpha < 0$ . Fig.(1.4) and fig.(1.5) to (1.6) show the real space boundary surfaces for ( $\mathbf{v0}$ ) and ( $\mathbf{v1}$ ) cases respectively. The boundary surfaces in fig.(1.4) are given by [ $\mathbf{2}^\circ : r^2 + z^2 = \nu_2/\beta$ ], [ $\mathbf{1}_\circ : r^2 + z^2 = (\nu_1 - \alpha\nu_2)/(1 - \alpha\beta)$ ], [ $\mathbf{2}_\circ : r^2 + z^2 = (\alpha\nu_1 - \nu_2)/(\alpha - \beta)$ ]. The boundary surfaces in fig.(1.5) are given by [ $\mathbf{1}^\circ : r^2 + r^{-2} + z^2 = \nu_1$ ], [ $\mathbf{2}^\circ : r^2 + z^2 = \nu_2/\beta$ ], [ $\mathbf{1}_\circ : (1 - \alpha\beta)(r^2 + z^2) + r^{-2} = \nu_1 - \alpha\nu_2$ ], [ $\mathbf{2}_\circ : (\alpha - \beta)(r^2 + z^2) + \alpha/r^2 = \alpha\nu_1 - \nu_2$ ]. Fig.(1.6) gives the structure of the mixture in the  $r$ - $z$  plane.

**Figure 2:** Typical ground state phase diagrams for ( $\mathbf{v0}$ )-**A** and ( $\mathbf{v0}$ )-**B**. We have chosen  $(\alpha = 0.9, \beta = 0.73)$  for **A**,  $(\alpha = 0.6, \beta = 0.73)$  for **B**. The dotted line in fig.(2.1) represents the case of equal particle numbers in both condensates,  $(N_1 = N_2)$ . As discussed in the text, for parameters appropriate for  $^{87}\text{Rb}$  and  $^{23}\text{Na}$ , and for current magnetic trap, we have  $N_1 = 16.7n_1, N_2 = 12.3n_2$ . The circle in fig.(2.1) indicate a mixture with  $N_1 = N_2 = 10^4$ . For the densities shown in fig.(2.3) to (2.9), the chemical potential  $\nu$  for the outer cloud is of the order of 10 to 20, giving rise to a mixture size of about 3 to 4 in dimensionless units, which is about  $2 \times 10^{-3}\text{cm}$  for a cloud of  $N_1 \approx 10^4, N_2 \approx 10^4$ .

**Figure 3:** Typical phase diagrams for ( $\mathbf{v1}$ ) and ( $\mathbf{v2}$ ) vortices for parameter range [**A** :  $0 < \alpha < 1, \beta < \alpha$ ], and [**B** :  $0 < \alpha < 1, \alpha < \beta$ ]. The values of  $(\alpha, \beta)$  used here are identical to those used in figure 2. Figures with letter labels “a”, “b”, etc. at the upper right corners show the boundary surfaces of the mixtures indicated by the same letter in the  $n_1$ - $n_2$  phase diagrams.

**Figure 4:** Fig.(4.1) shows the typical phase diagram for the ( $\mathbf{v1}$ ) vortices for case [**C**:  $\alpha < 0$ ], with  $(\alpha = -0.9, \beta = 0.73)$ . The notations here are identical to those in figure 3.



(1.3)

(1.4)

